European Journal of Pharmaceutical Sciences 111 (2018) 257–269

Contents lists available at ScienceDirect

European Journal of Pharmaceutical Sciences

journal homepage: www.elsevier.com/locate/ejps

Comparative evaluation of electrospraying and lyophilization techniques on solid state properties of Erlotinib nanocrystals: Assessment of *In-vitro* cytotoxicity

Shreya Thakkar[a], Dilip Sharma[b], Manju Misra[a,*]

[a] Department of Pharmaceutics, National Institute of Pharmaceutical Education and Research (NIPER), Ahmedabad, Gujarat 380054, India
[b] Department of Pharmacology and toxicology, National Institute of Pharmaceutical Education and Research (NIPER), Ahmedabad, Gujarat 380054, India

ARTICLE INFO

Keywords:
Lung cancer
Nanoprecipitation
Nanosuspension
Lyophilization
Electrospraying

ABSTRACT

Introduction: Erlotinib is a well known FDA approved drug from category of tyrosine kinase inhibitors; used for the treatment of lung cancer. However its use is limited because of its poor water solubility.
Objective: The aim of present work was to improve solubility by developing a stable nanocrystal based drug delivery system of ERL with the aid of sodium lauryl sulfate as potential stabilizer and to carry out comparative evaluation of electrospraying and lyophilization as solidification techniques on its solid state properties.
Experimental: Nanocrystal formulation was developed with antisolvent precipitation method having particle size, polydispersity index and zetapotential of 232.4 ± 4.3 nm, 0.162 and − 9.82 mV respectively. Further comparative evaluation of lyophilization and electrospraying was commenced as potential solidification techniques and solid powder matrix obtained from both the solidification techniques were compared in terms of size after re-dispersion (260 ± 4.8 and 329 ± 5.2 nm respectively), particle morphology, surface area (0.984 ± 0.11 and 0.341 ± 0.05 m^2/g respectively), pore volume (0.0014 and 0.0009 cc/g respectively), solid state of drug present and % drug release (~100% and ~78% respectively in 600 min). *In vitro* cytotoxicity studies shared that obtained formulation was having reduced IC50 values in comparison to drug. Further intracellular reactive oxygen species production was found to be higher for formulation treated cells when compared to free drug. Overall developed formulation was found to be potential drug delivery system for lung cancer therapy.

1. Introduction

Despite many recent advances reported for cancer therapy, lung cancer is still the most common and prevalent form of cancer reported worldwide. Recent cancer statistics reports, lung cancer to be most prevalent form of cancer (Around 224,390 newly diagnosed cases from 1,685,210 cases for all sites) in both males and females, associated with very high mortality rates (Miller et al., 2016; Siegel et al., 2016).

Drugs approved for lung cancer therapy extends from monotherapy using single drug candidates (Paclitaxel, docetaxel, methotrexate, gefitinib, bevacizumab, erlotinib hydrochloride, etoposide and others) to various combination therapies (carboplatin-taxol, gemcitabine-cisplatin) (https://www.cancer.gov/about-cancer/treatment/drugs/lung, https://www.cancer.org/cancer/non-small-cell-lung-cancer/treating/targeted-therapies.html). Protein kinase inhibitors, an important class of anticancer drug, which act by inhibiting the phosphorylation of amino acids, are gaining considerable attention as therapeutic agents these days (Roskoski, 2016; Zhang et al., 2009). One such class of protein kinase inhibitors is tyrosine kinase inhibitors, which act by competing with ATP for its binding site on the receptor, and ultimately inhibits the phosphorylation accompanying down-stream signaling pathways (Roskoski, 2016; Zhang et al., 2009). Erlotinib hydrochloride [N-(3-ethynylphenyl)-6,7-bis (2-methoxyethoxy) quinazoline-4-amine] (ERL) is well-known compound from the aforementioned category and is known to act on epidermal growth factor receptor (EGFR). It is approved drug candidate for use in non-small cell lung cancer along with

Abbreviations: ERL, erlotinib hydrochloride; SLS, sodium lauryl sulfate; ROS, reactive oxygen species; DCFH-DA, 2′, 7′-Dichlorodihydrofluorescein diacetate; MTT, 3-(4, 5-Dimethyl-2-thiazolyl)-2, 5-diphenyl-2H-tetrazolium bromide; PVP K-30, polyvinylpyrrolidone K-30; PVA, polyvinyl alcohol; DSC, differential scanning calorimetry; FTIR, fourier transform infrared spectroscopy; KBr, potassium bromide; PDI, polydispersity index; DCM, dichloromethane; CCDC, cambridge crystallographic data centre; DLS, dynamic light scattering; AFM, atomic force microscopy; PMMA, polymethyl methacrylate; DMSO, dimethyl sulfoxide; ANOVA, analysis of variance; ICH, international conference on harmonization; HSH, high shear homogenization; PXRD, powder X-ray diffraction

* Corresponding author.
E-mail address: manju@niperahm.ac.in (M. Misra).

http://dx.doi.org/10.1016/j.ejps.2017.10.008
Received 3 August 2017; Received in revised form 25 September 2017; Accepted 5 October 2017
Available online 06 October 2017
0928-0987/

advanced metastatic pancreatic cancer. ERL is also reported to be effective in the treatment of head and neck cancer, glioma and ovarian cancer (Truong et al., 2016). Regardless of ERLs potential for treatment of various cancers, its use is limited owing to its poor water solubility (BCS- class II) (Truong et al., 2016). ERL administered orally is only 60% bioavailable and moreover exhibits dose-dependent side effects such as rash, diarrhea, loss of appetite, erythematic and frontal alopecia. This further necessitates careful development of suitable drug delivery system to overcome these limitations associated with ERL and to deliver it in an effective manner.

Poor water solubility accounts for poor oral bioavailability and is one amongst the leading causes for failure of many drug candidates in drug discovery program. Numerous techniques are reported in literature to enhance water solubility of candidates falling under BCS class II such as co-crystals (Sugandha et al., 2014), use of co-solvents (Miyako et al., 2010), hydrotrophy (Maheshwari and Jagwani, 2011), micellar solubilization (Rangel-Yagui et al., 2005) and size reduction to nano scale (Hecq et al., 2005). All these techniques have their own advantages and limitations, few being, daily exposure limits of residual solvents permitted, toxicity of organic co-solvents (Klick and Sköld, 2004) and surfactants (Tadros, 2005) used.

Various techniques tried by researchers for enhancement of poor water solubility of aforementioned drug candidate (ERL) includes solid self-emulsifying formulation (Truong et al., 2016), nano-sponge technique (Dora et al., 2016), cyclodextrin complexation (Devasari et al., 2015) and amorphous solid dispersion (Huang, 2009). Commercially available innovator formulation of ERL (Tarceva®) marketed by a subsidiary of Roche, also contains sodium lauryl sulfate (SLS) as an important excipient for its solubilization (https://www.accessdata.fda.gov/drugsatfda_docs/label/2008/021743s010lbl.pdf).

In past few years, nanocrystallization approach for solubility enhancement has emerged as full-fledged technique to overcome the problem of poor water solubility. Ease of formulation and scale up has tremendously increased the popularity and acceptance of this technique, as is evident from several commercially available formulation based on drug nanocrystals (Junghanns and Müller, 2008). The drastic increase in solubility with nanocrystals is owing to very high surface area offered by them with a little aid of stabilizers (ionic, non-ionic and polymeric). Nanocrystals can be best transformed into oral products by various methods of solidification such as spray drying (Malamatari et al., 2016), lyophilization (Van Eerdenbrugh et al., 2008a; Van Eerdenbrugh et al., 2008b), pelletization (Van Eerdenbrugh et al., 2008b), and electro-spraying (Peltonen et al., 2010). Solidification techniques improve solid state stability of the nanocrystals and help to overcome compromised physical and chemical stability in case of liquid nanosuspensions, apart from retaining improved aqueous solubility offered by nanosuspensions.

In present work, we have formulated nanocrystal based formulation of ERL to counter its poor water solubility. Further lyophilization and electro-spraying techniques were evaluated in terms of their suitability to work as solidification technique for nanosuspension of ERL, in order to improve its stability. Both the techniques were compared further on the basis of different physicochemical properties like size after re-dispersion, particle morphology, surface area, pore volume, solid state of drug present and % drug release. Developed nanosuspension was compared with drug in terms of *in-vitro* cytotoxicity studies, observations of apoptotic cell death and production of intracellular reactive oxygen species (ROS).

2. Materials and methods

2.1. Materials

ERL was received as generous gift sample from Natco pharma Ltd. (Hyderabad, India). Mannitol, trehalose dihydrate, sucrose, 3-(4,5-Dimethyl-2-thiazolyl)-2,5-diphenyl-2H-tetrazolium bromide (MTT), 3,8-Diamino-5-[3-(diethylmethylammonio)propyl]-6-phenylphenanthridinium diiodide (propidium iodide), Hoecsht 33,342, 2′,7′-Dichlorodihydrofluorescein diacetate (DCFH-DA), Pluronic® F-127 and Pluronic® F-68 were obtained from Sigma-Aldrich (Germany). SLS, polyvinylpyrrolidone K-30 (PVP K-30), and polyvinyl alcohol (PVA) were products of HiMedia Laboratories (Mumbai, India). Sodium chloride, sodium hydroxide, disodium hydrogen phosphate and all other salts for buffer preparation were purchased from S D Fine Chemicals (Mumbai, India). All other solvents, reagents and chemicals used were of analytical grade. Water used in all the experiments was purified water from a Milli®-Q Biocel, Millipore® (USA) assembly.

2.2. Methods

2.2.1. Drug excipient compatibility studies

Physical and chemical compatibility of drug with various surfactants was evaluated using differential scanning calorimetry (DSC) (Mura et al., 2002), hot stage microscopy (Šimek et al., 2014) and Fourier transform infrared spectroscopy (FTIR) respectively. All the DSC measurements were carried out using Indium calibrated DSC 214 *polyma* (Netzsch, Germany) equipped with compressed air cooling system IC70. Data acquirement and analysis were carried out using *Proteus*® version 7.1 (Netzsch, Germany). The study was performed on ERL alone and (1:1) physical mixture of excipients with the drug. Samples (1–3 mg) were weighed into aluminum pans (Netzsch, Germany) and heated under dry nitrogen (50 ml/min) in the scanning range between 25 and 240 °C at a rate of 10 °C/min using empty pans as a reference.

For hot stage microscopy (Carl Zeiss microscope, Axiocam HRc and imager M2 m along with hot stage and temperature controller of Linkam, Germany) around 1–2 mg of physical mixture (1:1) was mounted on clean glass slide and cover slip was applied. Slide was loaded in hot stage setup and sample was scanned in the range of 25 to 240 °C at a rate of 10 °C/min to observe any changes occurring.

FTIR analysis was carried out using FTIR spectrometer equipped with QuickSnap™ DRIFT sampling module (FTIR ALPHA Bruker, Germany). Data acquisition and analysis were carried out using OPUS 7.5 software (Bruker, Germany). Briefly 4–5 mg of sample was triturated with moisture free potassium bromide (KBr) and pellet was made by the use of hydraulic press. This pellet was analysed after background correction with blank KBr pellet (background scan) in range of 400 to 4000 cm^{-1}.

2.2.2. Preparation of nanosuspension

Drug nanosuspension was formulated and optimized using bottom-up approach (nanoprecipitation) and combination techniques (nanoprecipitation technique followed by probe sonication). Nanoprecipitation was achieved using solvent-antisolvent method. Screening of solvents was done from methanol, ethanol, acetone, dichloromethane (DCM) and ethyl acetate. Stabilizers were evaluated form Pluronic® F-127, Pluronic® F-68, SLS, and PVP K-30. Various parameters affecting final size and polydispersity index (PDI) such as type of stabilizer, drug to stabilizer ratio, solvent to antisolvent ratio, rotational speed and processing time were optimized to achieve final parameters in acceptable range.

For combination approach using probe sonication; ERL nanosuspension obtained from nanoprecipitation step was further processed by probe sonication (Ultrasonic Processor VC505, Sonics & Materials, USA) for 5 min with processing conditions of 5 s impulse on, 3 s impulse off and amplitude of 25%. Another combination technique (nanoprecipitation with HSH) utilizes same process of nanoprecipitation followed by high shear homogenization (HSH) at 1500 rpm for 5 min.

Molecular modeling studies of ERL were done using Mercury software (Version 3.9) to have an idea of chemical groups projecting out from surfaces of unit cells, an important factor which may contribute significantly in selection of stabilizers. Parameters for unit cell and

atomic co-ordinates were acquired from Cambridge Crystallographic Data Centre (CCDC) using entry MIYBOM (CCDC identifier: 689,015). Unit cell generation and visualization was done using aforementioned software.

2.2.3. Solidification techniques for nanosuspension

Various solidification techniques like spray drying, freeze drying and others are used for solidification of nanosuspensions. Solid form is more desirable form, as reaction rates of physical and chemical interactions are faster in liquid state, in comparison to solid state. Two solidification techniques were evaluated for optimized batch *viz.* lyophilization and electro-spraying. Initial screening of various cryprotectants (mannitol, sorbitol, sucrose and trehalose dihydrate) for lyophilization (VirTis Genesis from SP scientific, USA) was done on the basis of freeze-thaw study. For preliminary studies, all the cryoprotectants were added in concentration of 10% and then various concentrations were optimized to have permitted values of S_f/S_i ratio (where, S_f and S_i are particle size after and before freeze-thaw cycles respectively). For freeze thaw studies cryoprotectants (various cryoprotectant) added nanosuspension were frozen at − 80 °C for 48 h, followed by thawing at room temperature. Two such freeze-thaw cycles were performed. After thawing, particle size and PDI of the nanosuspesnion were determined. The cryoprotectants giving S_f/S_i ratio of 1 ± 0.3 were selected for further optimization (Saez et al., 2000).

For setting the parameters of lyophilization cycle, preliminary assessment of cryoprotectant, T_g values was done using DSC. DSC was performed in a range of − 70 °C to 20 °C with a cooling and heating rate of 10 °C/min for all cryoprotectant solutions and a mixture of cryoprotectant with nanosuspension (Saez et al., 2000).

Electro-spraying (ESPIN NANO from physics equipment company, Chennai, India) of nanosuspension was performed by adding water soluble polymer (PVA) to ERL nanosuspension. Mannitol was further added in nanosuspension containing PVA to enhance the bulkiness and compressibility characteristics of electosprayed powder. Various processing parameters like polymer concentration, applied voltage, distance between collector and sprayer, flow rate and temperature were optimized to obtain free flowing ERL electrosprayed powder.

2.2.4. Formulation characterization

2.2.4.1. Analysis of particle size and zeta potential. Average particle size and PDI were measured by Malvern Zetasizer (Nano ZS90 series UK) working on the principle of dynamic light scattering (DLS). Samples were diluted before measurement to maintain count rate in range of 180–250 kcps. Zeta potential measurements were carried out using the same instrument. Measurements for nanosuspension were done as such, for lyophilized and electrosprayed powders, briefly 1 mg of product were redispersed in 5 ml of Milli®-Q water. Vortexing with sonication was done as per the need for uniform dispersion of sample. All the measurements were done in triplicate (n = 3).

2.2.4.2. Particle morphology. Analysis of particle morphology was done by optical microscopy and atomic force microscopy (AFM). Optical microscopy was performed with upright Carl Zeiss microscope utilizing Axiocam HRc camera with imager M2 m. Briefly small amount of sample was spread on glass slide and visualized under 100 × magnification. Images were taken in normal mode and birefringence mode to predict the nature of powder obtained (crystalline/amorphous).

AFM (Multimode 8, Bruker, USA) was performed in peak force tapping mode with typical resonance frequency of tip cantilever system for multimode 8 system. Samples were scanned at scan speed of 0.977 Hz and scan sizes set were in the range of 50 nm to 5000 nm. Sample preparation was done by diluting sample 100 times with Milli®-Q water and spreading onto the glass slide (1 cm × 1 cm). Prepared glass slides were allowed to dry at room temperature to avoid the movement of particles. Images were acquired in topographic and phase imaging mode with nanoscope analysis software.

2.2.4.3. Stability studies. Stability studies for nanosuspension was commenced by storing formulation at 4 °C and withdrawing samples at predetermined time points of day 3, 7, 10, 15, 20 and 30. Size and PDI value measurements for all the withdrawn samples was done with Malvern Zetasizer (Nano ZS90 series UK) with the same protocol mentioned in preceding sections. Studies were performed in triplicate (n = 3).

2.2.4.4. Physical state charaterization. The powder X-ray diffraction (PXRD) patterns were recorded by D8 Advance X-ray diffractometer (Bruker, Germany). Radiations generated from Cu-Kα source, filtered through Ni filter having a wavelength of 1.54 Å at 40 kV, 40 mA were used to study the X-ray diffracted pattern. The instrument was operated in continuous scan mode with a step size of 0.02 and step time of 0.2 s over the 2θ range of 3 to 40°. The recordings were made using 25 mm polymethyl methacrylate (PMMA) sample holder by placing an accurately weighed amount of samples (about 250 mg). Data acquisition and analysis was carried out using DIFFRACPLUS EVA (ver. 9.0) diffraction software.

2.2.4.5. Pore volume and surface area measurements. Pore volume and surface area measurement (Autosorb iQ3, Quantachrome instruments, USA) was done for electrosprayed and lyophilized powders to see the effect of these two processes on powder porosity. Briefly 9 mm round bottom sample holder was half filled with the sample and degassing was done at temperature of around 80 °C. After degassing sample analysis was done using glass rod added holder by dipping in liquid nitrogen cylinder. Data aquasition and analysis was done with ASiQwin software. Total surface area, pore size and pore volume were calculated with the help of software. All the measurements were taken in triplicate (n = 3).

2.2.4.6. Analysis of drug assay. Briefly 2 mg of both the lyophilized and electrosprayed powders were resuspended in water, diluted with methanol and analysed using reverse phase HPLC (Agilent 1200 infinity series equipted with open lab control software) method. C18 Kinetex® RP-HPLC column (250 mm × 4.6 mm, 5 µm) from Phenomenex (USA) was used for evaluation of samples. Samples were analysed using mobile phase composition of ammonium acetate buffer (pH 4.0) and acetonitrile in ratio of 50:50 with injection volume and flow rate of 20 µl and 1 ml/min respectively (Karunakara et al., 2012). All the samples were analysed at wavelength 247 nm using UV detector after filtering with syringe filter.

2.2.4.7. In-vitro release studies. Release studies for nanosuspension, physical mixture and drug were conducted using 0.1 N HCL + 1% SLS (https://www.accessdata.fda.gov/scripts/cder/dissolution/dsp_SearchResults.cfm) in 250 ml vessel maintained at 37 ± 1 °C at 100 rpm. Sink condition was maintained throughout the experiment. Release studies were conducted by suspending accurately weighed amount of the lyophilized powder, drug, physical mixture and electrosprayed powder in 0.1 N HCL + 1% SLS and transferring the same to dialysis membrane (submerged in release medium) having molecular weight cut off of 14 kDa. 5 ml of sample was withdrawn at predetermined time intervals and replaced with fresh media. Samples were withdrawn, diluted accordingly and analysed using HPLC method described previously. Experiments were conducted in triplicates (n = 3). Similarity factor was calculated using following equation.

$$f2 = 50\,Log\left\{\left[1 + \frac{1}{n}\sum_{t=1}^{n}(R_t - T_t)^2\right]^{-0.5} \times 100\right\}$$

where f2, n, R_t and T_t corresponds to similarity factor, number of dissolution points, dissolution values of reference and product respectively at time point t.

2.2.4.8. In-vitro cytotoxicity studies. Cytotoxicity studies were carried out on lung cancer cells (A549 cells). Cells were seeded in 96 well plates and were incubated for overnight in an atmosphere containing 5% CO_2 at 37 °C before their utilization for cell viability assay. Healthy cells without any drug or formulation treatment were taken as control. Formulation was compared with drug solution to have estimation of cell viability. On the day of treatment cells were treated with a range of drug concentrations (10 μM, 20 μM, 30 μM and 40 μM). Drug solutions of different concentrations were prepared in dimethyl sulfoxide (DMSO) with complete growth medium to have final concentration as 0.1% v/v DMSO. Formulation in the same way was diluted with complete growth medium to have concentrations of 10 μM, 20 μM, 30 μM and 40 μM. Treated cells were then incubated for 24 h in humidified atmosphere containing 5% CO_2 at 37 °C. On completion of incubation time period 20 μl of 5 mg/ml MTT solution was added and cells were further incubated for 4 h. Media was discarded and 150 μl of DMSO was added to dissolve formed formazan crystals of dark blue color. Absorbance of wells was taken at 570 nm using microplate reader (Multiskan™ GO, Thermo Scientific, Finland). Data acquisition and analysis was carried out using SkanIt software (generation 4).

2.2.4.9. Assessment of apoptosis. Hoecsht 33342 and propidium iodide double staining was used to identify cells undergoing early stages of apoptosis and dead cells. Propidium iodide is known to stain dead cells as red and Hoecsht 33342 stain provides detection of a cell undergoing early stage apoptosis (stained as blue) and cells undergoing death (bright blue color). Healthy cells without any drug or formulation treatment were taken as control. Cells were treated with different concentrations of drug and formulation as mentioned before. Media was discarded and cells were treated with fresh medium containing Hoechst 33,342 (1 μg/ml) and propidium iodide (5 μg/ml) incubated in 5% CO_2 at 37 °C for 20 min (Hu et al., 2007; Saito et al., 2001). After staining cells were observed under fluorescence microscope (Axio Vert.A1, Zeiss, Germany). Images were quantified by image J software.

2.2.4.10. Assessment of intracellular ROS production. Intracellular ROS was determined using DCFH-DA dye. This non-fluorescent dye permeates cells easily and gets hydrolyzed by esterase to DCFH. Peroxides from intracellular environment oxidize it to a fluorescent compound DCF (Shan et al., 2016; Sharma et al., 2016). Healthy cells without any drug or formulation treatment were taken as control. Cells were treated with different concentrations of drug and formulation as mentioned in preceding sections for 24 h and incubated. Media was replaced with fresh medium containing 20 μM DCFH-DA dye with further incubation of cells for 1 h. Cells were observed under fluorescence microscope (Axio Vert.A1, Zeiss, Germany). Images were quantified by image J software.

2.3. Statistical analysis

Statistical analysis was performed either by one way analysis of variance (ANOVA) or two way ANOVA by GraphPad PRISM® (version 5.01). Data is expressed as mean ± standard deviation ($n = 3$). Statistical significance was considered for values $P < 0.05$.

3. Results and discussion

3.1. Drug excipient compatibility studies

DSC curve of ERL showed an endothermic peak at 232 °C resembling the melting point of the drug (Barghi et al., 2012). The endothermic event of the drug was found to be retained in the range of 232 ± 10 °C for all the physical mixtures with stabilizers (Pluronic® F-68, Pluronic® F-127, SLS and PVP K-30) as shown in Fig. 1A. Some disturbances in endothermic peak was observed in presence of SLS; physical compatibility in this case was further studies with hot stage microscopy. Periodic images at various temperature intervals showed existance of drug particles till melting point without any change in appearance, indicating that SLS was not interacting with ERL. All the aforementioned surfactants were taken for further optimization of formulation.

FTIR analysis showed absorption bands at 3278 cm^{-1}, 1632 cm^{-1}, 1164 cm^{-1}, 1024 cm^{-1}, 940 cm^{-1} and 742 cm^{-1} (Shrawat et al., 2013) coresponding to O—H bond stretch of alcohols, N—H bending of amines, C—O bond stretch, =C—H bending and C—Cl stretch. No shifting of absorption bands for drug in presence of any surfactants (emergence of additional peaks for surfactants) was observed which confirms chemical compatibility of drug with surfactants used for further optimization process as shown in Fig. 1B.

3.2. Preparation of nanosuspension

Molecular modeling studies revealed that when ERL forms crystal, bulky hydrophobic groups and positively charged hydrogen are more likely to be oriented towards surface rather than in the interior part (Fig. 2). On the basis of this crystal visualization anionic and non-ionic/polymeric surfactants were presumed to be more appropriate for stabilization of ERL nanosuspension (Inacio et al., 2016). On the basis of drug stabilizer interaction study, SLS, Pluronic® F-68, Pluronic® F-127, and PVP K-30 were chosen for preparation of nanosuspensions.

Desired particle size and PDI of the final formulation were found to be dependent upon various parameters including solvent used, drug to surfactant ratio, solvent to antisolvent ratio, stirring speed and processing time (Sinha et al., 2013). One parameter was optimized at a time by keeping other parameters as constant. Ethanol, methanol, ethyl acetate, acetone and DCM were chosen as solvent for initial screening based on their miscibility with water and ERL solubility. Preliminary trials showed that DCM gave aggregated nanosuspension with larger particle size in comparison to ethanol, methanol, ethyl acetate and acetone which was probably due to slower diffusion of DCM in water, leading to less crystal nucleation and growth of larger particles (Lu et al., 2014). Specific values of size, PDI and zetapotential are listed in Table 1. Contrary to DCM; methanol, ethanol, acetone and ethyl acetate were giving nanocrystals of smaller size. Ethanol was selected as solvent of choice because of size and PDI of the obtained nanosuspension, which was in the optimum range. According to International conference on harmonization (ICH) guidelines for residual solvents ethanol is classified under class III solvents having limits of 5000 ppm/day and presents lesser risk to human health (Klick and Sköld, 2004).

The next important parameter affecting desired size and PDI was concentration of drug per ml. Drug concentration was varied from 0.2 mg/ml to 1 mg/ml. Results showed drug to be having limited solubility in ethanol also with clearly visible precipitate at concentration of 0.75 and 1 mg/ml. Final concentration of drug to be incorporated was selected as 0.5 mg/ml based upon the results obtained. Solvent to antisolvent ratio was optimized in the range of 1:2 to 3:5. Results suggested ratio of 3:5 to be suitable for preparation of nanocrystals probably owing to favoured conditions of supersaturation.

SLS, Pluronic® F-68 and Pluronic® F-127 were found to be giving size and PDI in range without any significant difference between values obtained in processing time of 15 min. Comparatively PVP K-30 was found to be giving higher particle size and PDI. SLS, Pluronic® F-68 and Pluronic® F-127 were taken further for optimization of other parameters. Drug to surfactant ratio was optimized for three stabilizers. For SLS, drug to surfactant ratio of 1:1 and 2:1 resulted in complete solubilization of nanocrystals and an unstable system having size in μm range. This could be due to the phenomenon of Ostwald ripening taking place leading to micellar solubilization of small particles along with growth of larger ones on expenses of small particles (Müller et al., 2001). Amount of SLS was further reduced to have ratio of 3:1; which resulted in acceptable size and PDI. Fig. 3 presents histogram and frequency curve of results obtained for size and zeta-potential

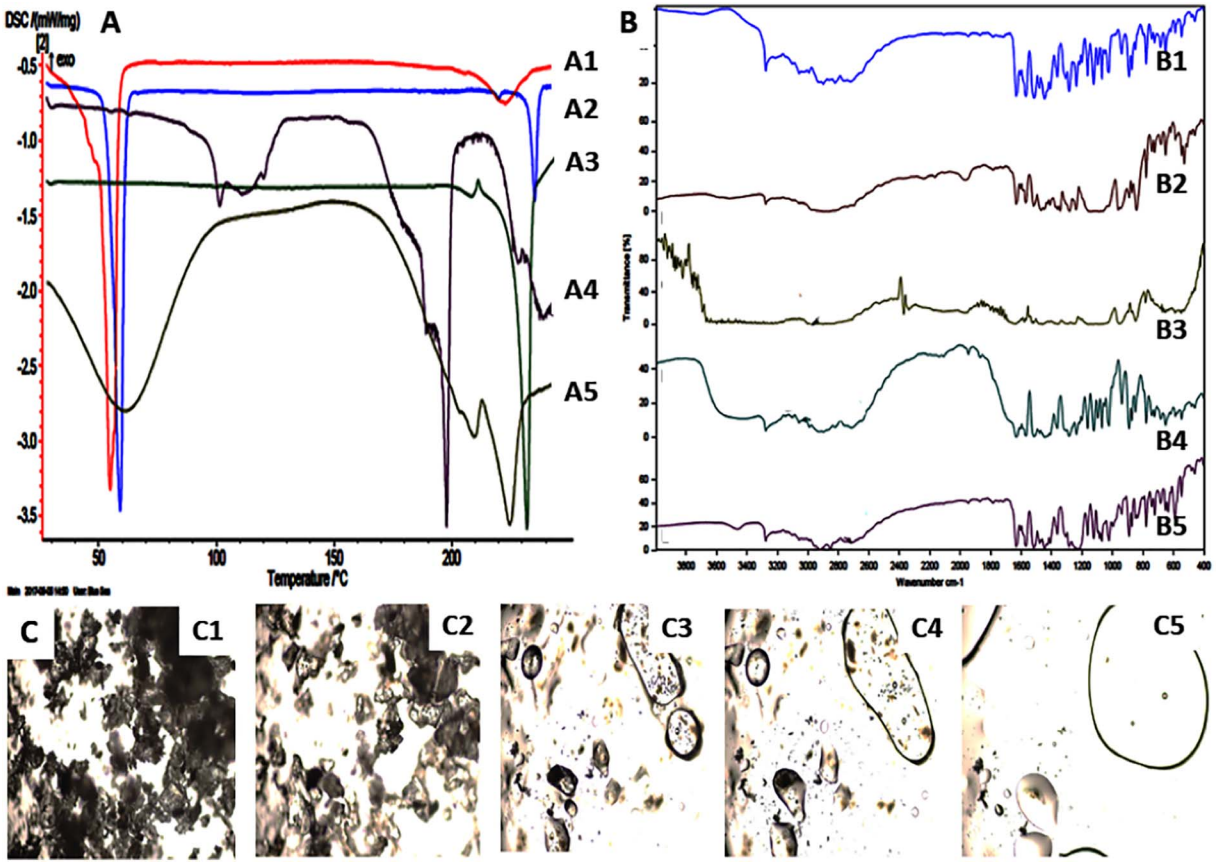

Fig. 1. A: DSC curves of, A1: Pluronic® F68 + ERL, A2: Pluronic® F127 + ERL, A3: ERL, A4: SLS + ERL, PVP K-30 + ERL. B: FTIR spectra of B1: ERL, B2: Pluronic® F68 + ERL, B3: Pluronic® F127 + ERL, B4: PVP K-30 + ERL, B5: SLS + ERL. C: Hot stage images of ERL with SLS at C1: 65 °C, C2: 95 °C, C3: 120 °C, C4: 150 °C, C5: 230 °C (All the images were taken at 100 × magnification).

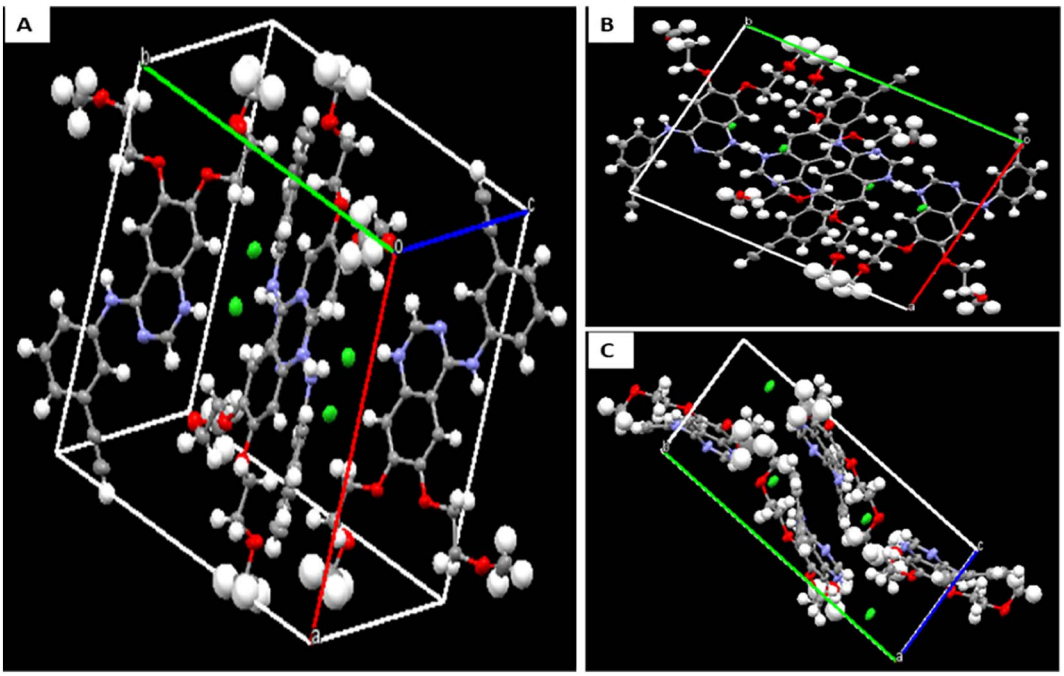

Fig. 2. Unit cells (containing 4 molecules of ERL) generated from the crystal structure using mercury software, A: Unit cell of ERL, B and C: Groups projecting out from different planes of unit cell. Colors scheme: C = grey, O = red, N = blue, H = white. (For interpretation of the references to color in this figure legend, the reader is referred to the web version of this article.)

Table 1
Specific values of size, PDI and zetapotential for various process parameters.

Nano-precipitation method			Average particle size (in nm)	PDI	Zetapotential (in mV)
Solvent		Methanol	1492 ± 98	1.0	− 1.9
		Acetone	965.7 ± 49	0.812	− 2.6
		DCM	5355.3 ± 68	1	− 1.3
		Ethanol	397.5 ± 14	0.356	− 4.2
		Ethyl acetate	249.9 ± 21	0.186	− 5.8
Drug concentration		0.2 mg/ml	228.3 ± 5.3	0.175	− 9.8
		0.5 mg/ml	234.9 ± 6.2	0.182	− 9.3
		0.75 mg/ml	Visible precipitate in ethanol only	–	–
		1 mg/ml	Visible precipitate in ethanol only	–	–
Solvent to anti-solvent ratio		3:5	250.1 ± 6.3	0.181	− 10.9
		1:2	498.7 ± 29	0.622	− 8.3
		1:3	Visible precipitate in 15 min processing	–	–
Stabilizer		Pluronic® F-68	243.0 ± 6.0	0.163	− 4.6
		Pluronic® F-127	220.6 ± 7.5	0.143	− 8.6
		SLS	225.1 ± 5.2	0.164	− 11.2
		PVP K-30	347.4 ± 9.8	0.215	− 2.9
Drug to stabilizer ratio	Drug: SLS	4:1	Visible precipitate	–	–
		3:1	229.5 ± 4.3	0.197	− 9.6
		2:1	Complete solubilization	–	–
		1:1	Complete solubilization	–	–
	Drug: Pluronic® F-68/Pluronic® F-127	1:7	239.1 ± 5.6	0.136	− 7.1
		1:10	Some % of particles in solubilized range	–	–
		1:15	Complete solubilization	–	–
Effect of stirring speed		600 rpm	224.6 ± 4.8	0.139	− 10.3
		800 rpm	1402.3 ± 38	0.909	− 9.3
		1000 rpm	1406.3 ± 81	0.960	− 8.7
Nano-precipitation + Probe sonication			Visible precipitate	–	–
Nano-precipitation + HSH			Visible precipitate	–	–

- Parameter not checked.

respectively. Further increase in ratio was associated with increased nanocrystal size; which could be attributed to insufficient amount of stabilizer required to stabilize nanocrystals formed. In case of nanosuspensions made with Pluronic® F-68 or Pluronic® F-127 drug to surfactant ratio of 1:7 was found to be suitable. Stirring speed was kept constant as 600 rpm on all aforementioned trials. It was observed that

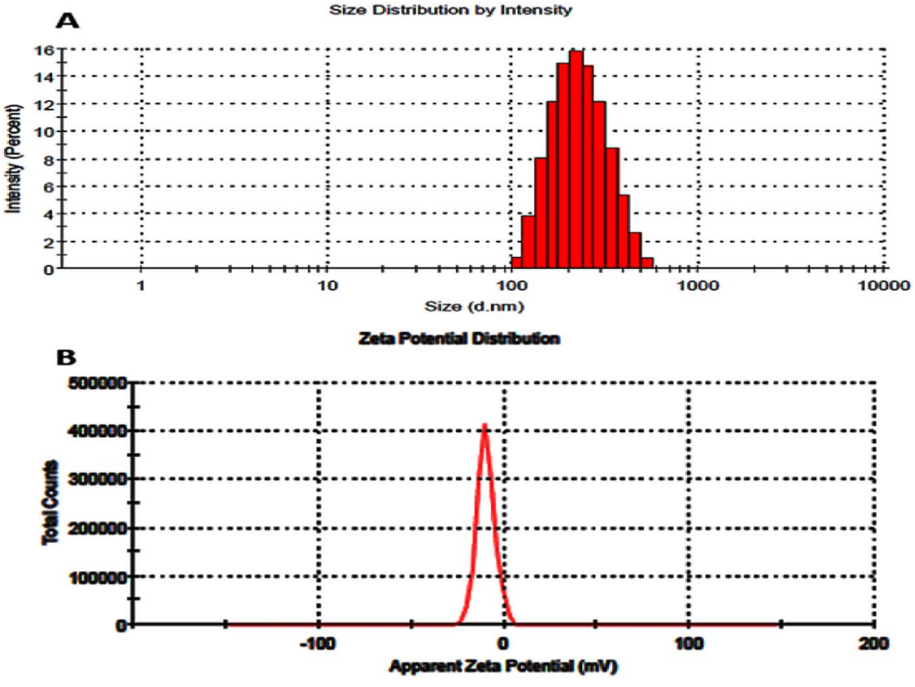

Fig. 3. Original histogram and frequency distribution curves of A: size and B: Zeta-potential for nanosuspension formulation.

increase in speed reduced processing time but resulted in non-reproducible results. On the basis of all the mentioned trials stirring speed of 600 rpm with processing time of 15 min was selected for optimized batches.

Apart from nanoprecipitation technique, two combination techniques *viz.*, probe sonication and HSH, were also used to further optimize the size of nanosuspension obtained, however both of these methods resulted in increased nanocrystal size and hence were not considered further. Increase in size could be attributed to energies provided by probe sonication and HSH process which are sufficient enough to initiate direct collision of particles or to overcome electrostatic/steric barriers generated with the use of stabilizers (Chu et al., 2006; Tso, 2010).

3.3. Solidification of nanosuspension to powder form

Amongst the cryoprotectants screened, Mannitol and sorbitol in concentration of 10% were found to give desired values of S_f/S_i ratio, when subjected to freeze thaw cycles. Further when the concentration of these two cryoprotectants was reduced to 2% and 5% level, system was not stable. It was observed that minimum 10% concentration of cryoprotectant, was needed to have desirable S_f/S_i ratio. Nanosuspensions stabilized with Pluronic® F-68 or Pluronic® F-127 showed further increase in S_f/S_i values after addition of cryoprotectants; and hence was not considered further. The finalized nanosuspension containing only SLS, was considered for further evaluation. Fig. 4 provides comparison of S_f/S_i values obtained with use of cryoprotectants in different concentrations.

T_g determination for cryoprotectants alone and in combination with nanosuspension (Table 3) suggested a small shift in values for almost all the cryoprotectants except sorbitol, which was an important factor governing lyophilization cycle. On the basis of lowest S_f/S_i and least shift in T_g values obtained, finally mannitol (in concentration of 10%) was selected as cryoprotectant of choice for lyophilization of nanosuspension.

To maintain similarity in composition of electrosprayed and lyophilized powders, mannitol was selected as an additive (bulking agent) of choice to be added in nanosuspension along with PVA for electrospraying. Concentration of PVA in final solution was optimized to be 1% in combination with 3.5% of mannitol. Increase in this concentration of PVA resulted in shift of process from electrospraying to electrospinning giving elastic nanofiber sheet, which was difficult to convert into free flowing powder, a feature, ideally desired for compression (Husain et al., 2016; Thakkar and Misra, 2017). Applied voltage, temperature and working distance were kept constant at values of 25 kV, 50 °C and 100 mm respectively to obtain easily scrap able free flowing electro sprayed powder.

Table 2
Specific values of size, PDI and zeta-potential for re-dispersed samples.

Sample	Size	PDI	Zeta-potential
Lyophilized powder	260 ± 4.8	0.201	− 5.6
Electrosprayed powder	329 ± 5.2	0.290	− 3.2

Table 3
T_g values of cryoprotectants in aqueous solution form and with nanosuspension.

Cryoprotectants	T_g of cryoprotectant solution (in °C)	T_g of cryoprotectant solution with nanosuspension (in °C)
Mannitol	− 31.6	− 32.8
Sorbitol	− 43.5	Not detected
Sucrose	− 35.6	− 39.7
Trehalose dihydrate	− 37.8	− 25.3

3.4. Formulation characterization

3.4.1. Analysis of particle size and zeta-potential

Specific values of particle size, PDI and zeta-potential for all the optimization batches are presented in Table 1. Values of particle size, PDI and zeta-potential for final batch prepared with SLS were 232.4 ± 4.3, 0.162 and − 9.82 respectively. Specific values of size, PDI and zeta-potential for re-dispersed lyophilized and electro-sprayed samples (~5 mg in 10 ml water) are given in Table 2.

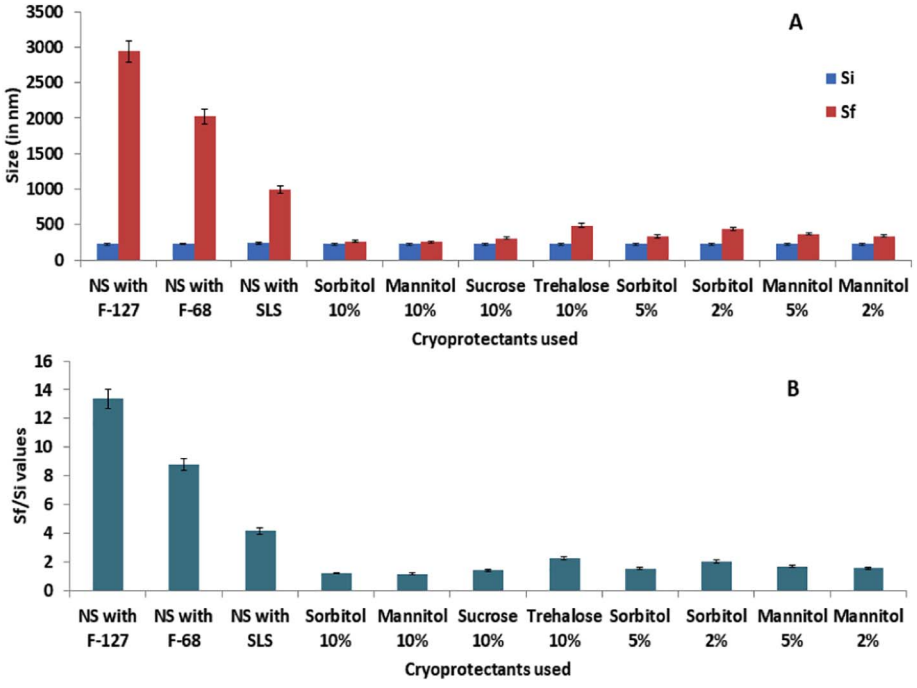

Fig. 4. A: Size of nanocrystals before (Si) and after (Sf) freeze thaw studies, B: Sf/Si ratio shown by various cryoprotectants in freeze thaw studies.

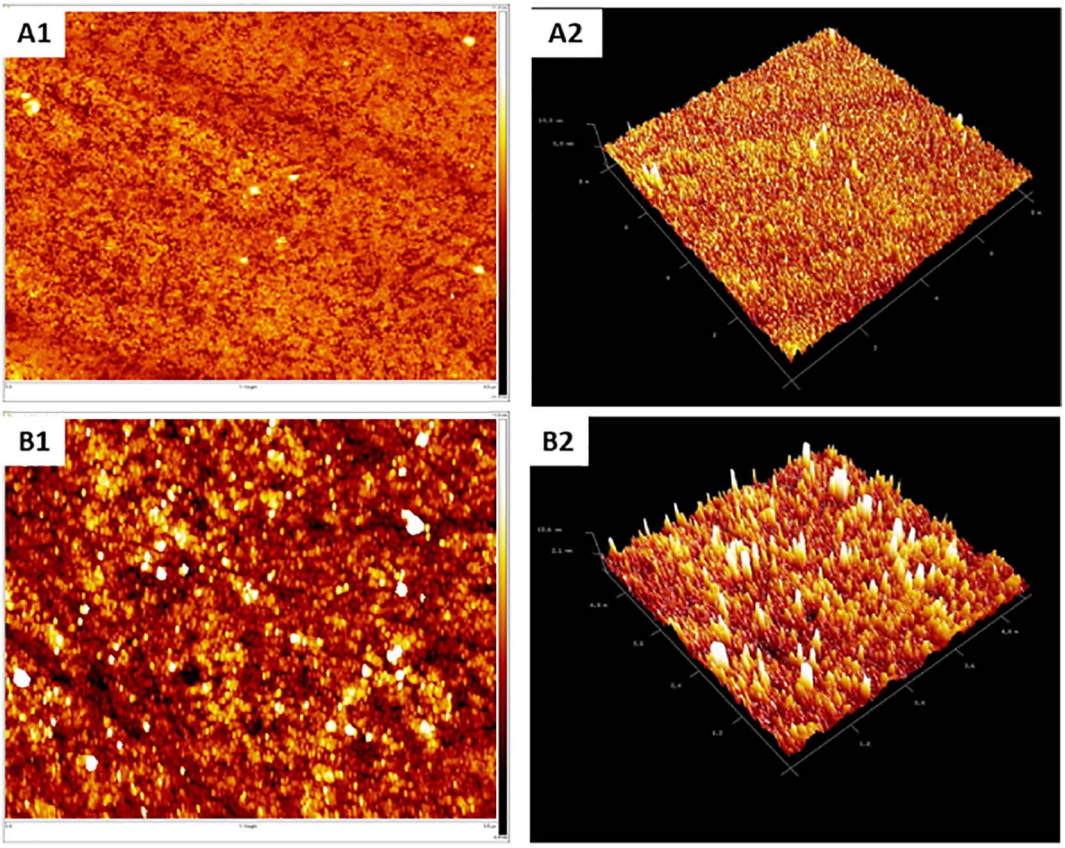

Fig. 5. AFM images of A: Nanosuspension and B: unprocessed drug.

3.4.2. Particle morphology

Images obtained by optical microscopy in birefringence mode (polarized light microscopy) for both the lyophilized and electro-sprayed powders showed crystalline nature confirmed by the birefringence as shown in Fig. 6C. Electro-sprayed powder was found to be showing less birefringence as compared to lyophilized powder which could be due to partial amorphization of sample by the presence of PVA. PXRD analysis was done to further confirm the results obtained from study.

AFM analysis was conducted to check any changes in surface roughness for nanocrystals as compared to unprocessed drug. Results suggested unprocessed drug to have particle size which was very high to detect with AFM and in the same way surface roughness for unprocessed drug was found to be ~40 nm. In contrast to this nanosuspension showed a size of ~300 nm with reduced roughness of 7.4 nm as shown in Fig. 5. Results were in accordance to study conducted by Gao et al. which reported a reduction in surface roughness for smaller size nanocrystals of drug amitriptyline hydrochloride as compared to larger size agglomerates (Gao et al., 2013).

3.4.3. Physical state characterization

DSC curves obtained for lyophilized powder showed well separated endothermic events for β-D-mannitol and drug at 167.2 °C and 215.8 °C respectively. This depression in melting point of drug could be attributed either to reduced particle size or good miscibility of drug with excipients used. Shete et al. in the same way have reported melting point depression for nanocrystalline drug formulated with excipients having good miscibility (Shete et al., 2015). On the other hand electrosprayed powder showed three defined peaks at 153.0 °C, 167.2 °C and 221.3 °C corresponds to endothermic events for δ-D-mannitol, β-D-mannitol and drug respectively. Some researchers have reported conversion of β form of mannitol to δ and α forms after some processing conditions as these forms are known to nucleate first (before β form) (Cornel et al., 2010; Fronczek et al., 2003; Shete et al., 2015). Further researchers have reported no significant difference between heat of solubilization for these (Burger et al., 2000).

XRD analysis revealed characteristic peaks of drug at 2θ values of 5.8, 10.54, 19.06, 24.3, 26.2 and 28.1 (Jyothi Prasad et al., 2010) suggesting drug to be present in crystalline form as shown in Fig. 7. Lyophilized powder showed presence of all the peaks at specific 2θ values showing drug to retain its crystalline form. In case of electrosprayed powder intensity of all the peaks were found to be decreased which could be due to partial amorphization of drug. It is well reported that polymeric excipients having properties of water solubility enhancement are often associated with amorphization of content by virtue of interfering with nucleation and crystal growth. Some polymers are also reported to have high configurational entropy due to their flexible structure which allows them to exist in many conformations resulting in reduced free energy of amorphous form (Baghel et al., 2016). Results obtained from polarized light microscopy were in accordance with PXRD data.

FTIR analysis of lyophilized and electrosprayed powders displayed retention of all characteristic absorption bands for drug along with emergence of new bands for excipients.

3.4.4. Stability studies

Drug nanosuspension was found to be stable at 4 °C with slight increase in size. Study was conducted for a time period of 3 months and sampling at various time point suggested little increase in size and PDI over the time period of study as shown in Fig. 8.

3.4.5. Pore volume and surface area measurement

Study was conducted in order to give some idea regarding release profile as higher surface area and highly porous samples generally results in higher release rates (Fonte et al., 2012). Lyophilized and

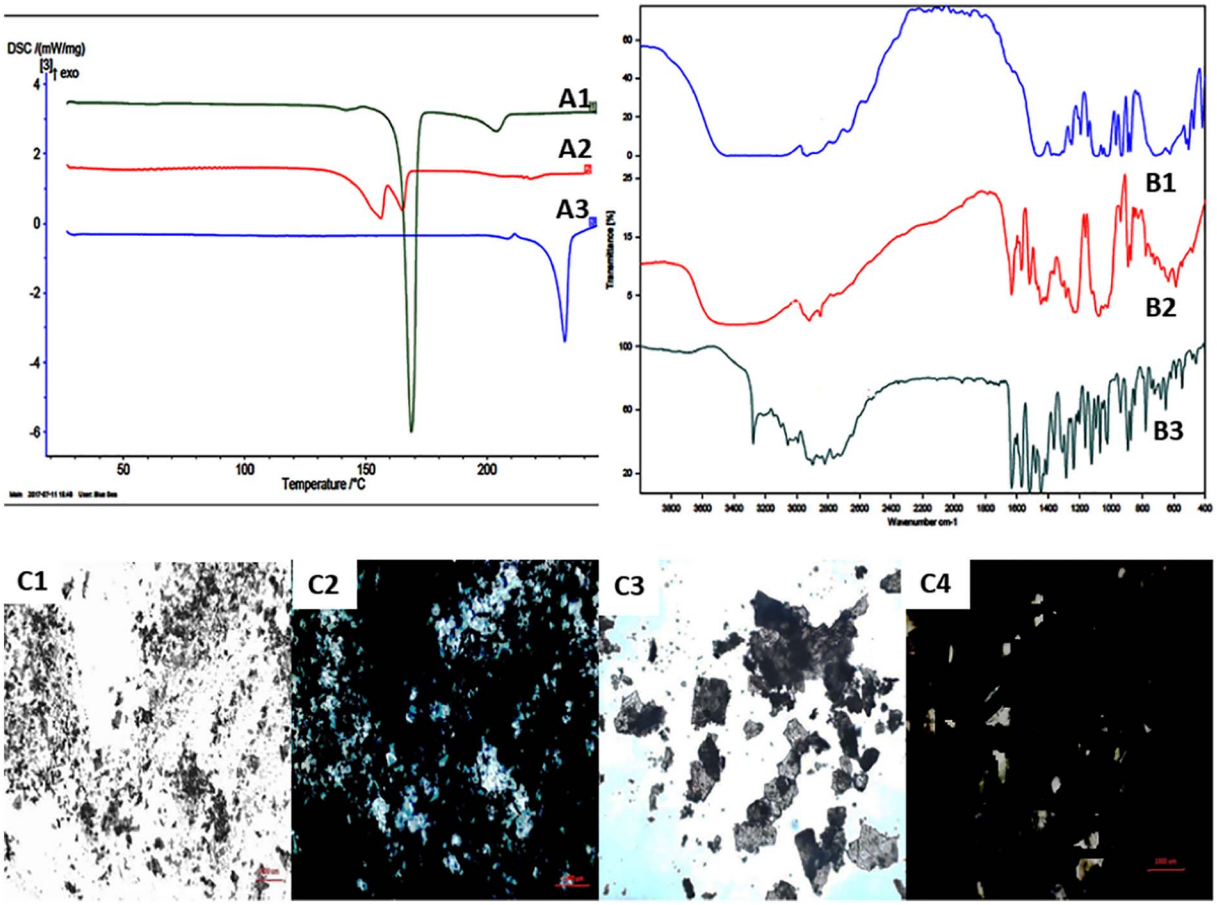

Fig. 6. A: DSC curves of A1: lyophilized powder, A2: Electrosprayed powder and A3: ERL; B: FTIR spectra of B1: Lyophilized formulation, B2: Electrosprayed formulation and B3: ERL; C: Optical microscopic images of C1: Lyophilized sample, C3: Electrosprayed sample in normal mode and C2: Lyophilized sample, C4: Electrosprayed sample in polarized mode.

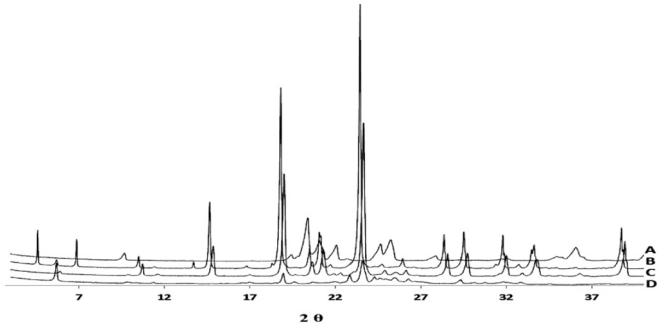

Fig. 7. XRD spectra of A: Electrosprayed powder, B: Physical mixture, C: Lyophilized sample, D: ERL.

electro-sprayed powders were found to be showing an increase of 6 and 3 fold in surface area (Fig. 9) as compared to physical mixture alone. Data was further correlated with cumulative % release. Significant enhancement ($P < 0.001$) for surface area was found in case of lyophilized powder in comparison to physical mixture whereas electrosprayed powder resulted in non-significant values for surface area enhancement ($P < 0.05$).

3.4.6. Amount of drug present in powder matrix

Assay of drug for lyophilized powder was found to be 95.3% while electro-sprayed powder resulted in assay value of 78.5% which is quite lower in comparison to lyophilized powder. Probable reason could be the material loss during collection of electro-sprayed powder from collector on which it is deposited.

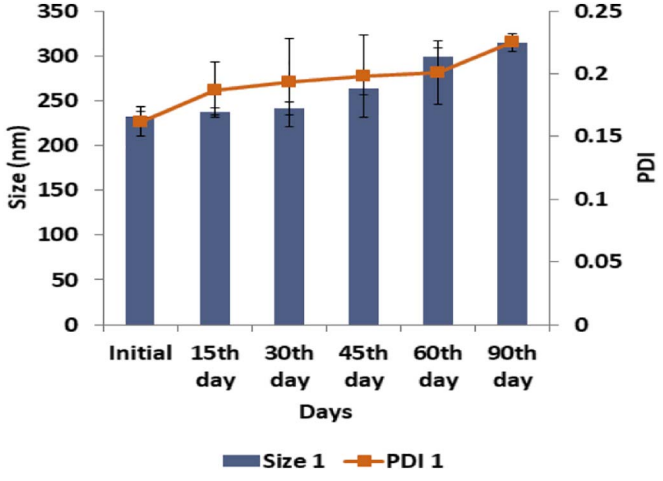

Fig. 8. Stability studies conducted at 4 °C for one month. Each data point is expressed as the mean ± SD ($n = 3$).

3.4.7. In-vitro release studies

Data obtained from released studies showed physical mixture and drug to be having non-significant difference ($P < 0.05$) between their release profiles. Both the lyophilized powder and electrosprayed powder of drug nanocrystals showed significant ($P < 0.001$) enhancement in release profile as compared to drug and physical mixture. Lyophilized powder showed better release profile than electrosprayed samples (lyophilized powder ~ 100% cumulative release in 600 min as

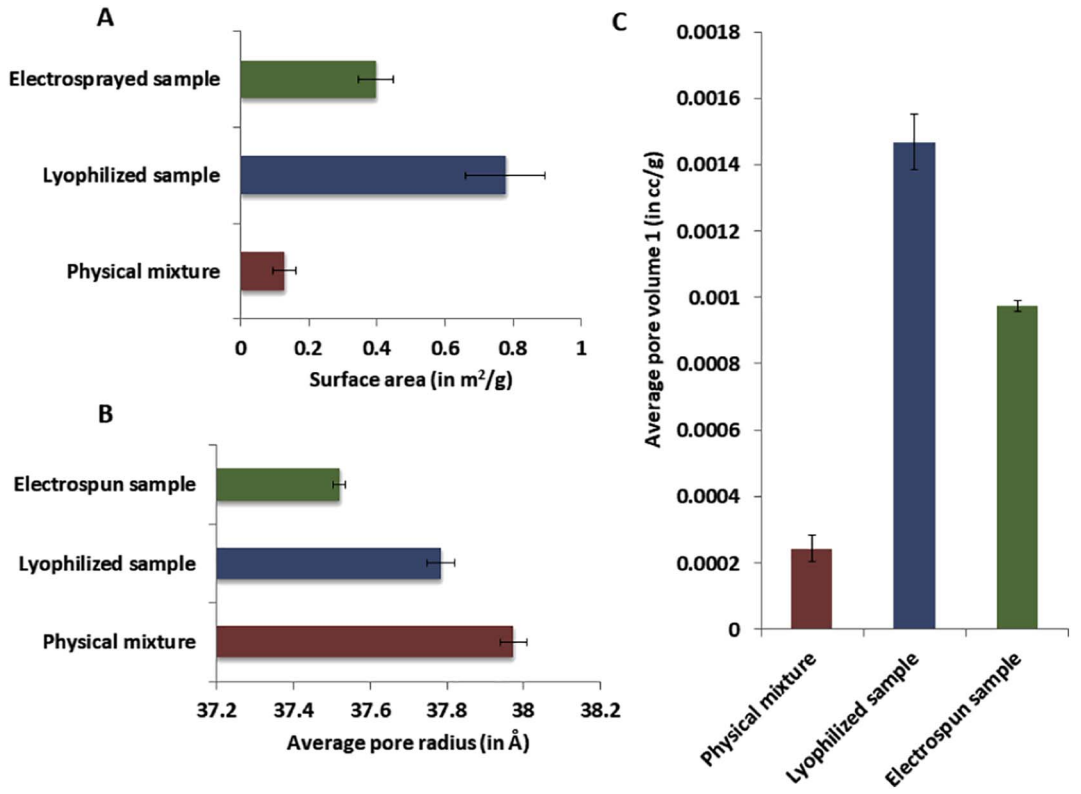

Fig. 9. A: Surface area of samples (in m^2/g), B: Average pore size for sample particles (in Å), C: Average pore volume for sample particles (in cc/g). Each data point is expressed as the mean ± SD (n = 3).

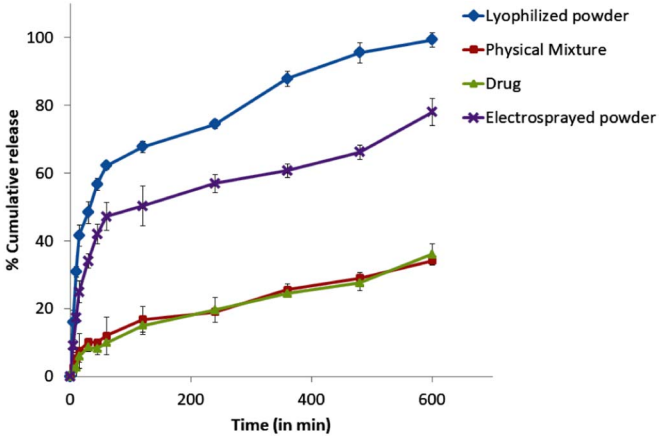

Fig. 10. Release profile for lyophilized sample, electrosprayed sample, physical mixture and drug respectively. Each data point is expressed as the mean ± SD (n = 3).

compared to electrosprayed powder which resulted in only ~78% cumulative release in the same time frame (Fig. 10). Results obtained from release studies, very well correlated with findings of surface area measurements; as lyophilized powder showed higher surface area and hence higher % of cumulative drug release. Further release profiles of lyophilized and electro-sprayed powders were compared with unprocessed drug by applying similarity factor. Values obtained for similarity factor of lyophilized and electro-sprayed powders were 18.37 and 27.34 respectively. Similarity factor based comparison showed release profiles to be significantly different from that of unprocessed drug as values obtained were < 50.

3.4.8. In-vitro cytotoxicity studies

Cytotoxicity studies were carried out in A549 cells to assess cell inhibitory activity of developed formulation with respect to free drug.

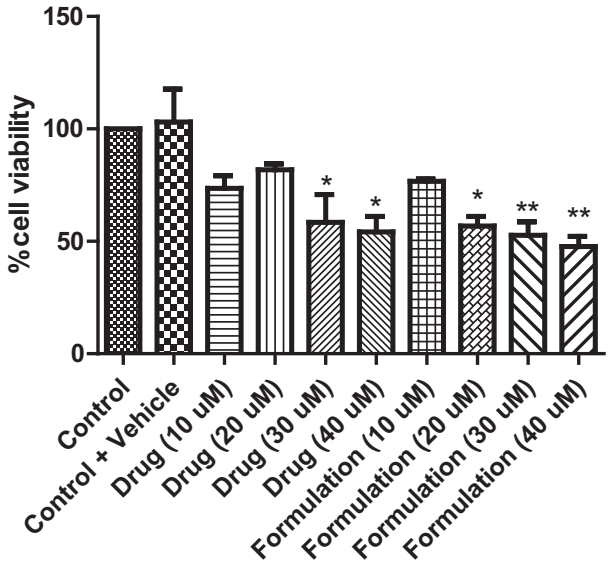

Fig. 11. % cell viability of A549 cells treated with different concentrations of drug and formulation (0, 10, 20, 30 and 40 μM). Observations suggest higher concentrations of drug (30 and 40 μM) to produce significant effect on cell viability, $P < 0.05$ in comparison to control. In case of formulation even lower concentration of 20 μM found to show significant effect, $P < 0.05$ as compared to control. Results are expressed as percentage of cell viability content in various groups compared to control. All values are expressed in mean ± SEM, $n = 9$ wells from three independent experiments. $^{**}p < 0.01$; $^{*}p < 0.05$ *versus* control.

Percantage cell viability was calculated after treatment with various concentrations of drug and formulation (0, 10, 20, 30, 40 μM). Observations suggest decrease in % cell viability in concentration dependent manner (for both drug and formulation). The inhibitory concentration (IC50) values for free drug and nanosuspension was found to

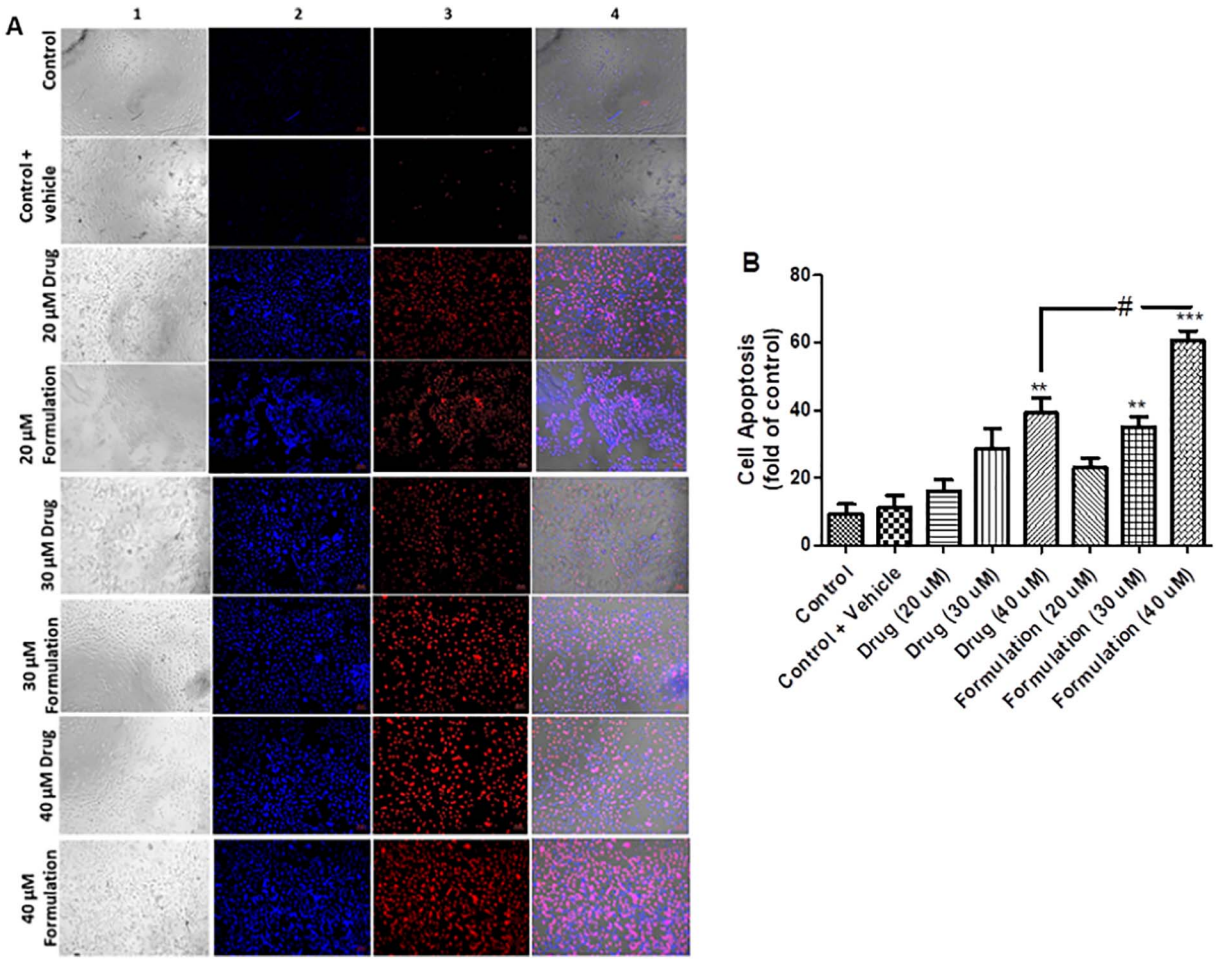

Fig. 12. Effect of ERL on apoptosis of A549 cells. Cells were treated with different concentrations of drug and formulation (0, 10, 20, 30 and 40 µM). Level of apoptosis was observed after Hoecsht 33,342/propidium iodide double staining in A549 cells; cells in early stage of apoptosis (stained blue) and apoptotic dead cells (red stain). Images were taken with fluorescence microscope (scale bar: 20 µm). (A) 1: bright field images, 2: images of cells stained with Hoecsht 33,342, 3: Images of cells stained with propidium iodide and 4: merged images. (B) Bar graph showing comparison of drug and formulation on cell apoptosis in different concentrations. Results are expressed as apoptotic cells in various groups as compared to control and each other. All values are expressed in mean ± SEM, n = 9 wells from three independent experiments. ***$P < 0.001$; **$P < 0.01$ as compared to control; $^{\#}$ $P < 0.05$ *vs.* drug (40 µM). (For interpretation of the references to color in this figure legend, the reader is referred to the web version of this article.)

be 29.37 ± 3.74 and 20.14 ± 0.92 respectively (Fig. 11). Formulation was found to be showing better cell inhibitory activities with respect to drug especially upon increasing dose. However, the difference between drug and formulation was significant at higher ratios only which could be attributed to attainment of saturation solubility of formulation in limited media volume available.

3.4.9. Assessment of apoptosis

Apart from *in-vitro* cytotoxicity studies Hoecsht 33,342/propidium iodide double staining was done to observe cells in early stages of apoptosis and apoptotic cell death. This double staining is known for staining cells, blue which are in early stages of apoptosis and the cells which died due to apoptosis as red. Images obtained for cells treated with different concentrations of drug and formulation showed number of apoptotic cell death was proportional to concentration of drug available for action. Results obtained were in accordance to results of MTT assay, showing higher cell apoptosis for cells treated with formulation as compared to drug. Significant difference was found for higher concentrations as shown in Fig. 12.

3.4.10. Determination of intracellular ROS production

DCF fluorescence was found to be increased with increase in drug concentration available for showing action. As shown in Fig. 13 Intracellular ROS levels were significantly increased for A549 cells treated with higher concentrations of drug as well as formulation. Effect of formulation on ROS production was higher as compared to free drug which could be attributed to higher concentration of drug available from nanosuspension owing to fast drug release.

4. Conclusion

Stable nanosuspension of ERL was developed using SLS as stabilizer having particle size, PDI and zeta-potential values of 232.4 ± 4.3 nm, 0.162 and − 9.82 mV respectively. Comparative evaluation of lyophilization and electrospraying technique as solidification techniques on the basis of amount of drug present, size after re-dispersion, particle morphology, surface area, pore volume, solid state of drug present and % drug release revealed superiority of lyophilized powder over electrosprayed powder. Nanosuspension as such was found to be stable at 4 °C for 3 months. *In-vitro* cytotoxicity studies for free drug and nanosuspension showed IC50 values of 29.37 ± 3.74 and 20.14 ± 0.92 respectively. Intracellular ROS production was found to be higher in cells treated with formulation with respect to drug. Overall developed delivery system has shown potential for enhancing apparent solubility of drug. Further powders obtained by drying techniques can be utilized in formation of tablet dosage form after addition of some excipients. *In-vivo* studies will be undertaken in near future to evaluate and confirm advantage offered by developed formulation.

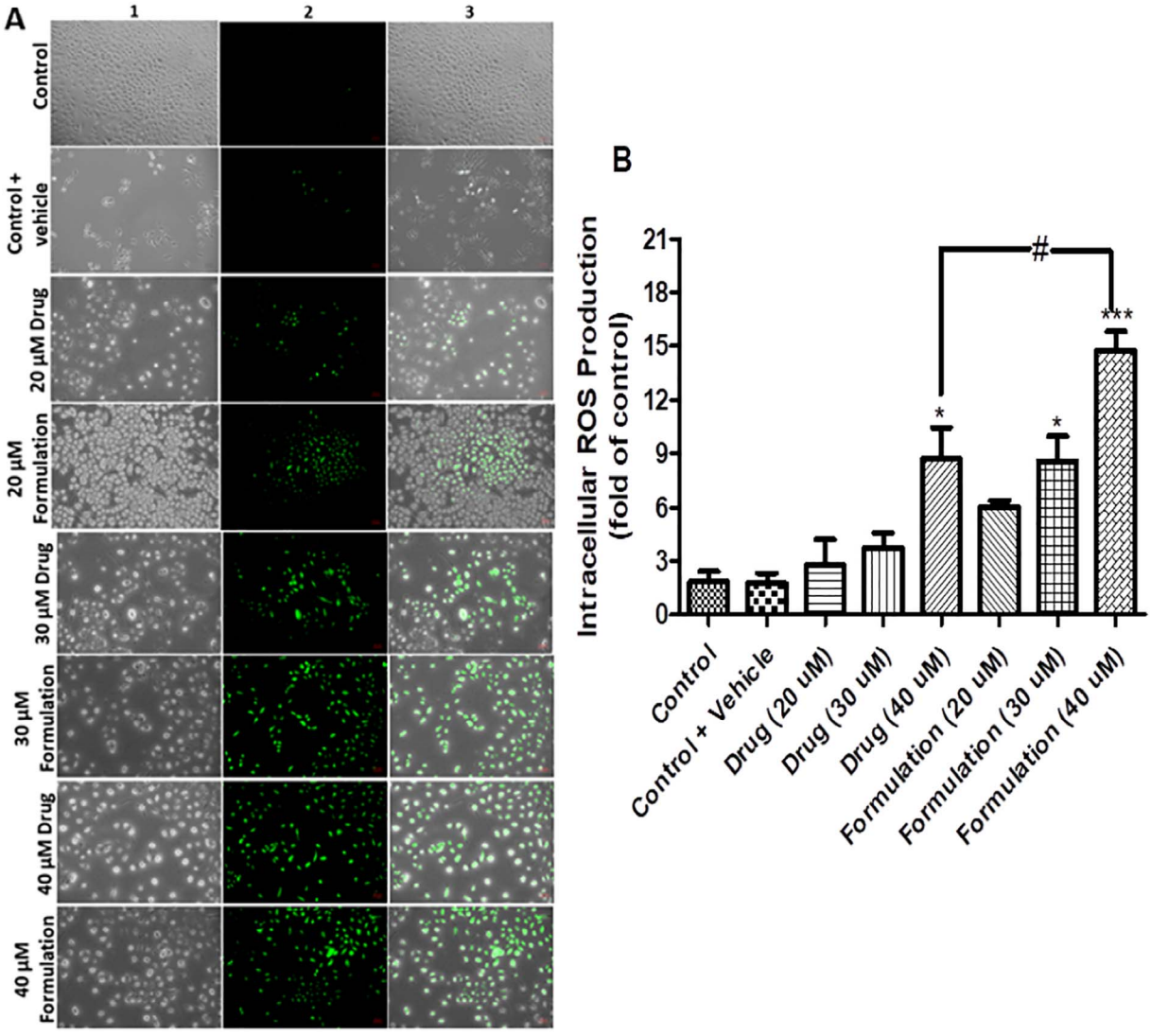

Fig. 13. Effect of ERL on intracellular ROS production of A549 cells. Cells were treated with different concentrations of drug and formulation (0, 10, 20, 30 and 40 μM). Level of intracellular ROS production was observed after staining with DCFH-DA dye in A549 cells. Images were taken with fluorescence microscope (scale bar: 20 μm). (A) 1: bright field images, 2: images of DCF fluorescence, 3: merged images. (B) Bar graph showing comparison of drug and formulation on cell ROS production in different concentrations. Results are expressed as ROS production in various groups as compared to control and each other. All values are expressed in mean ± SEM, n = 9 wells from three independent experiments. ***P < 0.001; *P < 0.05 as compared to control; # P < 0.05 *vs.* drug (40 μM).

Acknowledgement

Authors are thankful to Department of pharmaceuticals, ministry of chemicals and fertilizers, Government of India, for providing financial assistance to Shreya in form of PhD Fellowship. Authors would like to acknowledge Natco pharma Ltd. (Hyderabad, India) for providing Erlotinib as a generous gift sample and to Cadila pharmaceuticals Pvt. Ltd. (Ahmedabad, India) for providing support in lyophilization process.

Conflict of interest

Authors report no conflict of interest.

References

[02.06.2017] Available from. https://www.cancer.gov/about-cancer/treatment/drugs/lung.
[02.06.2017] Available from. https://www.cancer.org/cancer/non-small-cell-lung-cancer/treating/targeted-therapies.html.
[04/06/2017] Available from. https://www.accessdata.fda.gov/drugsatfda_docs/label/2008/021743s010lbl.pdf.
[25/06/2017] Available from. https://www.accessdata.fda.gov/scripts/cder/dissolution/dsp_SearchResults.cfm.
Baghel, S., et al., 2016. Polymeric amorphous solid dispersions: a review of amorphization, crystallization, stabilization, solid-state characterization, and aqueous solubilization of biopharmaceutical classification system class II drugs. J. Pharm. Sci. 105, 2527–2544.
Barghi, L., et al., 2012. Modified synthesis of erlotinib hydrochloride. Adv. Pharm. Bull. 2, 119–122.
Burger, A., et al., 2000. Energy/temperature diagram and compression behavior of the polymorphs of D-mannitol. J. Pharm. Sci. 89, 457–468.
Chu, S.-H., et al., 2006. Ultrasonication of bismuth telluride nanocrystals fabricated by solvothermal method. Proc. SPIE 1–8.
Cornel, J., et al., 2010. Precipitation and transformation of the three polymorphs of d-mannitol. Ind. Eng. Chem. Res. 49, 5854–5862.
Devasari, N., et al., 2015. Inclusion complex of erlotinib with sulfobutyl ether-β-cyclodextrin: preparation, characterization, in silico, in vitro and in vivo evaluation. Carbohydr. Polym. 134, 547–556.
Dora, C.P., et al., 2016. Potential of erlotinib cyclodextrin nanosponge complex to enhance solubility, dissolution rate. In: Vitro Cytotoxicity and Oral Bioavailability. 137. Carbohyd. Polym., pp. 339–349.
Fonte, P., et al., 2012. Effect of cryoprotectants on the porosity and stability of insulin-loaded PLGA nanoparticles after freeze-drying. Biomatter 2, 329–339.
Fronczek, F.R., et al., 2003. Three polymorphs (α, β, and δ) of D-mannitol at 100 K. Acta Crystallogr. C 59, 567–570.
Gao, B., et al., 2013. A novel preparation method for drug nanocrystals and characterization by ultrasonic spray-assisted electrostatic adsorption. Int. J. Nanomedicine 8,

3927–3936.
Hecq, J., et al., 2005. Preparation and characterization of nanocrystals for solubility and dissolution rate enhancement of nifedipine. Int. J. Pharm. 299, 167–177.
Hu, Z., et al., 2007. Synthesis of β-alanine C 60 derivative and its protective effect on hydrogen peroxide-induced apoptosis in rat pheochromocytoma cells. Cell Biol. Int. 31, 798–804.
Huang, L., 2009. Amorphous Form of Erlotinib Hydrochloride and its Solid Amorphous Dispersion.
Husain, O., et al., 2016. Investigating the particle to fibre transition threshold during electrohydrodynamic atomization of a polymer solution. Mater. Sci. Eng. C 65, 240–250.
Inacio, R., et al., 2016. Investigating how the attributes of self-associated drug complexes influence the passive transport of molecules through biological membranes. Eur. J. Pharm. Biopharm. 102, 214–222.
Junghanns, J.-U.A., Müller, R.H., 2008. Nanocrystal technology, drug delivery and clinical applications. Int. J. Nanomedicine 3, 295–310.
Jyothi Prasad, R., et al., 2010. Novel Polymorphs of Erlotinib Hydrochloride and Method of Preparation. United States. (US20100261738 A1).
Karunakara, C., et al., 2012. Separation and determination of process-related impurities of erlotinib using reverse-phase HPLC with a photo-diode array detector. Anal. Sci. 28, 305.
Klick, S., Sköld, A., 2004. Validation of a generic analytical procedure for determination of residual solvents in drug substances. J. Pharm. Biomed. 36, 401–409.
Lu, Y., et al., 2014. Development and evaluation of transferrin-stabilized paclitaxel nanocrystal formulation. J. Control. Release 176, 76–85.
Maheshwari, R., Jagwani, Y., 2011. Mixed hydrotropy: novel science of solubility enhancement. Indian. J. Pharm. Sci. 73, 179–183.
Malamatari, M., et al., 2016. Solidification of nanosuspensions for the production of solid oral dosage forms and inhalable dry powders. Expert Opin. Drug Deliv. 13, 435–450.
Miller, K.D., et al., 2016. Cancer treatment and survivorship statistics, 2016. CA cancer. J. Clin. Densitom. 66, 271–289.
Miyako, Y., et al., 2010. Solubility enhancement of hydrophobic compounds by cosolvents: role of solute hydrophobicity on the solubilization effect. Int. J. Pharm. 393, 48–54.
Müller, R., et al., 2001. Nanosuspensions as particulate drug formulations in therapy: rationale for development and what we can expect for the future. Adv. Drug Deliv. Rev. 47, 3–19.
Mura, P., et al., 2002. Compatibility studies of multicomponent tablet formulations. DSC and experimental mixture design. J. Therm. Anal. Calorim. 68, 541–551.
Peltonen, L., et al., 2010. Electrospraying, spray drying and related techniques for production and formulation of drug nanoparticles. Expert Opin. Drug Deliv. 7, 705–719.
Rangel-Yagui, C.O., et al., 2005. Micellar solubilization of drugs. J. Pharm. Sci. 8, 147–163.
Roskoski, R., 2016. Classification of small molecule protein kinase inhibitors based upon the structures of their drug-enzyme complexes. Pharmacol. Res. 103, 26–48.
Saez, A., et al., 2000. Freeze-drying of polycaprolactone and poly (D,L-lactic-glycolic) nanoparticles induce minor particle size changes affecting the oral pharmacokinetics of loaded drugs. Eur. J. Pharm. Biopharm. 50, 379–387.
Saito, T., et al., 2001. β-Amyloid induces caspase-dependent early neurotoxic change in PC12 cells: correlation with H2O2 neurotoxicity. Neurosci. Lett. 305, 61–64.
Shan, F., et al., 2016. Erlotinib induces the human non–small-cell lung cancer cells apoptosis via activating ROS-dependent JNK pathways. Cancer Med. 5, 3166–3175.
Sharma, D., et al., 2016. Effects of 4-phenyl butyric acid on high glucose-induced alterations in dorsal root ganglion neurons. Neurosci. Lett. 635, 83–89.
Shete, G., et al., 2015. Oral bioavailability and pharmacodynamic activity of hesperetin nanocrystals generated using a novel bottom-up technology. Mol. Pharm. 12, 1158–1170.
Shrawat, V.K., et al., 2013. Crystalline Erlotinib Hydrochloride Process United States. (US20150299141 A1).
Siegel, R.L., et al., 2016. Cancer statistics, 2016. CA cancer. J. Clin. Densitom. 66, 7–30.
Šimek, M., et al., 2014. Hot-stage microscopy for determination of API particles in a formulated tablet. Biomed. Res. Int. 2014.
Sinha, B., et al., 2013. Bottom-up approaches for preparing drug nanocrystals: formulations and factors affecting particle size. Int. J. Pharm. 453, 126–141.
Sugandha, K., et al., 2014. Solubility enhancement of ezetimibe by a cocrystal engineering technique. Cryst. Growth Des. 14, 4475–4486.
Tadros, T.F., 2005. Surfactants in pharmaceutical formulations. In: Applied Surfactants: Principles and Applications, pp. 433–501.
Thakkar, S., Misra, M., 2017. Electrospun polymeric nanofibers: new horizons in drug delivery. Eur. J. Pharm. Sci. 107, 148–167.
Truong, D.H., et al., 2016. Development of solid self-emulsifying formulation for improving the oral bioavailability of erlotinib. AAPS Pharm. Sci. Tech. 17, 466–473.
Tso, C.-p., et al., 2010. Stability of metal oxide nanoparticles in aqueous solutions. Water Sci. Technol. 61, 127–133.
Van Eerdenbrugh, B., et al., 2008a. Alternative matrix formers for nanosuspension solidification: dissolution performance and X-ray microanalysis as an evaluation tool for powder dispersion. Eur. J. Pharm. Sci. 35, 344–353.
Van Eerdenbrugh, B., et al., 2008b. Top-down production of drug nanocrystals: nanosuspension stabilization, miniaturization and transformation into solid products. Int. J. Pharm. 364, 64–75.
Zhang, J., et al., 2009. Targeting cancer with small molecule kinase inhibitors. Nat. Rev. Cancer 9, 28–39.